Absolute rate coefficient measurements of the reactions of vibrationally cold HD+ and H3+ ions with neutral C atoms

Florian Grussie, Lukas Berger, Manfred Grieser, Ábel Kálosi, Damian Müll, Oldřich Novotný, Aigars Znotins, Fabrice Dayou, Xavier Urbain, Holger Kreckel

Editors' Suggestion | Featured in Physics

Absolute rate coefficient measurements of the reactions of vibrationally cold HD^+ and H_3^+ ions with neutral C atoms

Florian Grussie,[1] Lukas Berger,[1] Manfred Grieser,[1] Ábel Kálosi,[2,1] Damian Müll,[1] Oldřich Novotný,[1] Aigars Znotins,[1] Fabrice Dayou,[3] Xavier Urbain,[4] and Holger Kreckel[1,*]

[1]*Max-Planck-Institut für Kernphysik, Saupfercheckweg 1, 69117 Heidelberg, Germany*

[2]*Columbia Astrophysics Laboratory, Columbia University, New York, New York 10027, USA*

[3]*Sorbonne Université, Observatoire de Paris, PSL University, CNRS, LERMA, F-92195 Meudon, France*

[4]*Institute of Condensed Matter and Nanosciences, Université catholique de Louvain, B-1348 Louvain-la-Neuve, Belgium*

(Received 8 December 2023; accepted 2 April 2024; published 10 June 2024)

Ion-neutral reactions are driving the formation of small molecules in the gas phase of interstellar clouds, where hydrogen molecules and their ions are by far the most important collision partners for any species in the astrochemical network. Here we present absolute rate coefficient measurements for the reactions $HD^+ + C \rightarrow CH^+/CD^+ + D/H$ and $H_3^+ + C \rightarrow CH^+/CH_2^+ + H_2/H$ obtained using a recently commissioned ion-neutral collision setup at the Cryogenic Storage Ring. Our measurements with vibrationally cold ions result in significantly higher rate coefficients when compared with previous studies using internally excited ions, bringing them in better agreement with classical capture theories. Moreover, we have performed detailed quasiclassical trajectory (QCT) calculations for the $HD^+ + C$ reaction, using new potential energy surfaces. Our experimental results and the QCT calculations show very good agreement for the absolute cross section of the reactions, as well as for the isotope effect. These results have great potential relevance for the chemistry of the interstellar medium and the onset of organic chemistry in space.

DOI: 10.1103/PhysRevA.109.062804

I. INTRODUCTION

Ion-neutral reactions are an important class of processes in a variety of fields. Driven by the attractive potential between the induced dipole of the neutral reactant and the charge of the ion, these reactions often proceed rapidly even under extreme conditions, e.g., in the cold interstellar medium [1] or in ionized regions of planetary atmospheres [2]. A number of different techniques have been employed throughout the years to study ion-neutral collisions, most of them based on flow tubes at room temperature [3]. A limited number of reactions have been studied at lower temperatures in uniform supersonic flows [4,5], with recently upgraded experiments using an ion selector before introducing the ions into the flow reactor [6,7]. Another type of experiment applies buffer gas cooling in cryogenic ion traps to thermalize the reactants by collisions with inert gases [8]. For an overview and comparison of various techniques see Ref. [9].

A particularly difficult type of ion-neutral processes for studies in the laboratory are reactions between molecular ions and neutral atoms. In this case both collision partners are very reactive and need to be carefully prepared in defined quantum states for meaningful experiments (see Refs. [10,11] for reviews). Since essentially all elements in the periodic table (apart from the noble gases) are in molecular form under terrestrial conditions, the production of neutral atoms requires some molecular dissociation process. For example, H, O, and N can be extracted in monoatomic form from microwave discharges of the molecular parent gases, and introduced into flow tubes. This technique has been used to study a number of processes involving these atoms [11], albeit restricted to measurements at room temperature. Furthermore, reactions between C atoms and various neutral molecules have been measured in room-temperature low-pressure flow experiments [12], while both inelastic and reactive collisions between C atoms and various molecules have been studied in supersonic flow reactors [13–15] and in dedicated velocity map imaging experiments [16].

A more versatile type of experiments, allowing for energy-resolved studies, employ the merged beams method. Coming at the expense of increased experimental complexity, initial merged beams studies were often limited to atomic collision partners [17–22], while a number of molecular systems have been addressed by single-pass experiments [23–25], with a recent emphasis on astrochemical reactions [26–28]. For example, the reaction between H_3^+ and C has been measured in a merged beams study [26] that found the rate coefficient for the formation of CH^+ to be a factor of ∼3 below the classical Langevin value. A recommended thermal rate was derived from this experiment and astrophysical implications were examined [29]. Furthermore, a combined experimental

*holger.kreckel@mpi-hd.mpg.de

and theoretical study of the reactions of internally excited H_2^+ and D_2^+ ions with C atoms by Hillenbrand *et al.* [30] found that the experimental cross sections were about a factor of ∼4 lower than standard capture theories, taking into account either the charge-induced dipole interaction potential or the combined charge-quadrupole and charge-induced dipole interaction potentials. Both of these previous studies were carried out with internally excited molecular ions that were extracted from standard electron impact ion sources.

We have recently commissioned the first merged beams setup for ion-neutral reactions at a heavy-ion storage ring [31]. This experiment allows for energy-resolved measurements of reactions between ground term atoms and stored molecular ions, which have time to cool to the vibrational ground state and also undergo some rotational cooling during storage. The setup is located at the Cryogenic Storage Ring (CSR) of the Max Planck Institute for Nuclear Physics in Heidelberg, Germany. Here, we present absolute rate coefficient measurements for reactions of C atoms with vibrationally cold HD^+ and H_3^+ ions. In both cases we find the experimental rate coefficients for vibrationally cold ions to be clearly enhanced compared to the single-pass studies using hot ions, and to be much closer to the expected classical capture rates.

Furthermore, we present theoretical studies of the $HD^+ + C$ collision system in Sec. III A, employing quasiclassical trajectory calculations on new CH_2^+ reactive surfaces. These calculations show excellent agreement with our experimental results, indicating that the present type of exothermic ion-neutral reaction can indeed be described and understood in detail using largely classical arguments.

II. EXPERIMENTAL SETUP AND MERGED BEAMS PRINCIPLE

The design and the operational features of the Cryogenic Storage Ring (CSR) have been described in an earlier publication [32]. In brief, the CSR is a fully electrostatic storage ring with a circumference of 35.1 m. Its ion optical lattice is able to store positive and negative particle beams with kinetic energies of up to 300 keV per unit charge. The CSR vacuum system employs a nested structure with inner ultra-high vacuum chambers surrounded by a large cryostat. During operation, the inner vacuum chambers of the CSR are cooled to cryogenic temperatures of $\leqslant$5 K by a closed-cycle helium refrigerator. Detailed photodissociation and photodetachment studies have shown that infrared-active molecular ions cool to their lowest rotational states within a few minutes of storage inside the CSR [33–35]. The cryogenic temperatures result in a very low residual gas density on the order of 10^3 particles per cubic centimeter. Two independent high-voltage platforms are used to supply ion beams to the CSR and adjacent experiments.

A. Ion-neutral merged beams measurements

A dedicated ion-neutral merged beams setup for the CSR has been constructed recently [31]. The experiment features a laser neutralization zone to create velocity-matched atomic neutral beams that can be superimposed to the stored ions in one of the straight sections of the storage ring. The neutral beam traverses the CSR ballistically, before it is disposed of in an extraction beam line downstream of the interaction region, where the neutral flux can be monitored continuously by secondary electron emission. Several dedicated detectors are used to record the charged reaction products at various ports inside the CSR or at the end of the extraction beam line. Details on the ion-neutral setup and proof-of-principle experiments of reactive collisions between D_2^+ ions and ground-term C atoms forming CD^+ ions can be found in a recent publication [31].

For the present work, the molecular ions are produced in a discharge source, mass selected by a dipole magnet, and electrostatically accelerated to a kinetic energy of 40 keV. For the experiments with HD^+ ions, we utilized HD gas inside the ion source. The measured reaction channels for the reaction of HD^+ with C atoms are

$$HD^+ + C \rightarrow CH^+ + D, \tag{1a}$$

$$\rightarrow CD^+ + H. \tag{1b}$$

The HD gas was ionized by electron impact and we suppressed the production of triatomic molecular ions by operating the ion source with a minimum amount of gas. However, by repeated scans of the mass range from 1–6 atomic mass units, we found that a small contamination (<5%) of the HD^+ beam with triatomic hydrogen ions was inevitable. Since H_3^+ also reacts with C, this will lead to the following reaction channels:

$$H_3^+ + C \rightarrow CH^+ + H_2, \tag{2a}$$

$$\rightarrow CH_2^+ + H, \tag{2b}$$

which result in the same product masses (within the resolution of our experiment) as the $HD^+ + C$ reaction. Therefore, we also measured the rate coefficient of vibrationally cold H_3^+ reacting with C as a function of the relative collision energy, and we will use these data to correct the measured rate coefficients for the contribution resulting from the H_3^+ contamination. For these experiments we operated the ion source with H_2 gas.

We stored approximately 2×10^8 HD^+ (H_3^+) ions at a kinetic energy of 40 keV inside the CSR, and we observed a typical initial $1/e$ beam lifetime around ∼15 s for both beams. While beams of heavier molecules with higher kinetic energy can exhibit much longer lifetimes [32], faster decays are to be expected in this case. The comparatively low energy of the stored beams makes them more susceptible to voltage fluctuations of the electrostatic deflectors, and the large number of stored ions in the present experiments introduces additional loss processes, in particular at short storage times, where space charge effects play a role.

The neutral C atom beam was superimposed to the stored ions in the same straight section of the CSR that is also used for the ion beam injection. The C atoms were produced by laser neutralization of a fast C^- anion beam. The negative carbon ions were extracted from a standard metal-ion sputter source (MISS), mass selected by a set of dipole magnets, accelerated to 161 keV, and guided toward the CSR. On their path to the storage ring, the C^- ions traversed a 2.9 m long photodetachment cell, where they are collimated by round apertures with 4.5 mm diameter. In this chamber, the anions are exposed to the field of a strong (1.8 kW) continuous diode laser array operating at a wavelength of 808 nm. The laser is

superimposed to the ion beam at a grazing angle of 2.7 degrees to increase the beam overlap (to an effective overlap length of roughly 20 cm) and thus boost the neutralization efficiency (see previous publication for details [36]). A fraction of about ∼2% of the fast anions is neutralized and enters the CSR on an essentially straight (ballistic) trajectory, while the remaining anions are deflected into a Faraday cup, where their current is recorded. Upon exiting the CSR, the neutral beam enters an extraction beam line downstream of the interaction zone, where it is eventually dumped in a neutral cup that uses secondary electron emission to monitor the neutral flux [31].

Photodetachment through the infrared laser light will produce only C atoms in the ^{3}P ground term, while we expect the fine structure sublevels to be occupied statistically [28,37]. The laser (and thus the neutral beam) can be switched with kilohertz frequencies, and we typically turn it on and off with a period of 6 ms (166 Hz) during the measurements for background subtraction.

The relative collision energy E_r for two nonrelativistic particle beams that intersect at an angle θ with kinetic energies E_1, E_2 and masses m_1, m_2, respectively, is given by

$$E_r = \frac{1}{2}\mu \mathrm{v}_r^2 = \mu\left[\frac{E_1}{m_1} + \frac{E_2}{m_2} - 2\left(\frac{E_1 E_2}{m_1 m_2}\right)^{\frac{1}{2}}\cos\theta\right], \quad (3)$$

where $\mathrm{v_r}$ denotes the relative velocity and μ the reduced mass [$\mu = m_1 m_2/(m_1 + m_2)$]. In our case, we aim for a colinear arrangement ($\cos\theta = 1$) and we vary the relative collision energy by changing the neutral beam kinetic energy. To this end the photodetachment takes place inside a drift tube that can be biased with voltages from −5 to +5 kV. For the present experiment, we chose fixed kinetic energies of 40 keV for the stored ions and 161 keV for the C^- beam. With these values velocity matching was achieved at a drift tube voltage of −1 kV (neutral beam energy of 160 keV), and we were able to cover relative collision energies of up to 10 eV in the center-of-mass frame, without changing the platform voltage for the C^- beam.

The charged reaction products (CH^+, CD^+, or CH_2^+), which, owing to their large kinetic energy compared to the stored HD^+ or H_3^+ ions, will experience only a small deflection by the electrostatic 6° deflector downstream of the interaction region, are deflected back into the neutral beam by a parallel deflector and leave the storage ring into the neutral extraction beam line [31]. Here, the ions are separated from the neutral beam by electrostatic fields, mass selected by a set of two large 55° energy analyzers, and eventually recorded as individual particle events by a channel electron multiplier (CEM) detector. The background-subtracted product count rate S is typically smaller than $10\,\mathrm{s}^{-1}$, and the CEM has a near-unity detection efficiency at the energies used here, while exhibiting a dark count rate below $0.1\,\mathrm{s}^{-1}$.

We measure the merged beams rate coefficient $k(E_r)$ as a product of the reaction cross section σ and the distribution of the relative velocities $\mathrm{v_r}$. It is given by

$$k(E_r) = \langle \sigma\, \mathrm{v}_r \rangle = \frac{S}{T_p \eta}\frac{e^2}{I_\mathrm{C}\, I_{\mathrm{M}^+}}\frac{\mathrm{v_C}\,\mathrm{v_{M^+}}}{L\langle\Omega(z)\rangle}, \quad (4)$$

where S denotes the product count rates in the CEM detector (for CH^+/CD^+ or CH^+/CH_2^+ ions); T_p stands for the product transmission of the extraction beam line; η is given by the detection efficiency of the CEM detector; $\mathrm{v_C}$ and $\mathrm{v_{M^+}}$ represent the velocities of the C atoms and the molecular ions (HD^+ or H_3^+), respectively; and L denotes the length of the interaction region with an average merged beams overlap form factor along the interaction zone $\langle\Omega(z)\rangle$ [31]. The current attributed to the circulating ions is given by I_{M^+}. As in previous merged beams studies [21,22,26,31,38], we artificially assign one elementary charge e to each neutral atom and treat the neutral flux as a current I_C.

To evaluate $\langle\sigma v_r\rangle$ on an absolute scale, all the parameters on the right-hand side of the Eq. (4) need to be known or recorded during the measurement. Our setup allows us to determine all of the required quantities within reasonable uncertainties during the experiment. However, as the determination of the overlap factor $\Omega(z)$ is time consuming and introduces the largest uncertainty for the absolute scale of our measurements [31], we decided to make use of the fact that the particle trajectories inside the electrostatic ion optical lattice of the CSR, and thus the ion beam profiles, are independent of the particle mass for the same kinetic energy. We measured the known rate coefficient for the reaction of $C + D_2^+ \rightarrow CD^+ + D$ during the same experimental campaign in order to normalize our data to previous measurements, and thus significantly reduce the overall systematic uncertainty. A full account of the error budget for the present study is given in Sec. II C.

B. Characterization of relative collision energies

In any experiment with merged or crossed beams, it is imperative to understand the distribution of the relative collision energies, as it typically differs from a thermal distribution. Furthermore, in the sections where the two beams are merged and demerged, higher relative collision energies will be sampled as the beams are not collinear. The resulting angle leads to increased relative velocities, which need to be accounted for.

To this end we have performed simulations of the beam trajectories of the stored ion beam and the overlapping neutral atom beam. Using the finite-element code TOSCA OPERA3D [39], the precise field maps for all ion-optical elements were calculated. These field maps serve as a basis for the G4BEAMLINE code [40], which allows us to simulate the trajectories of individual particles (see also Ref. [31]). The neutral atom beam is defined by two round apertures (with a diameter of 4.5 mm at a distance of 2.9 m from one another) in the transfer beam line before entering the CSR. As a result, the neutral atom beam exhibits a 2σ emittance of ∼1.4 mm mrad inside the CSR. For the stored ion beam, we assume an emittance of $\epsilon_{x,y}(2\sigma) \sim 10$ mm mrad, which we routinely observe in our experiments with uncooled beams when storing $\sim 10^8$ particles.

Monte Carlo simulations of these beams (neutral beam and stored ion beam) overlapping in the first straight section of the CSR were performed. Recording the velocity vectors of the particles along the ion-neutral interaction region, allows for the determination of the relative collision energy E_r. By varying the kinetic energy of the neutral particles for each simulation, we can infer the distribution of the relative collision energy for all measured data points. As discussed in detail

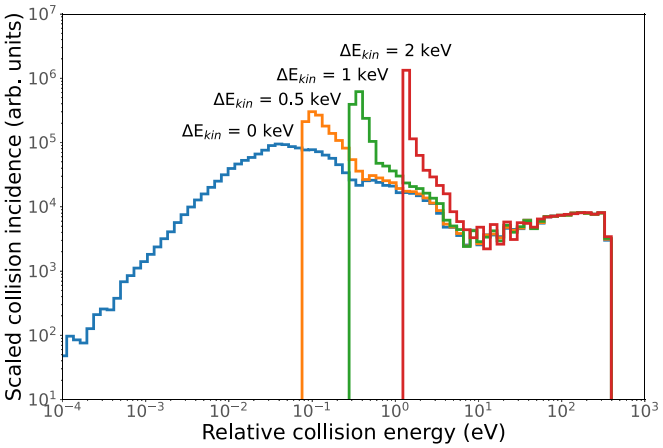

FIG. 1. Distributions of the relative collision energies for various detuning energies of the neutral C atom beam. The distributions were derived from Monte Carlo simulations of both beams (see main text for details). Bins are of equal width on a logarithmic scale.

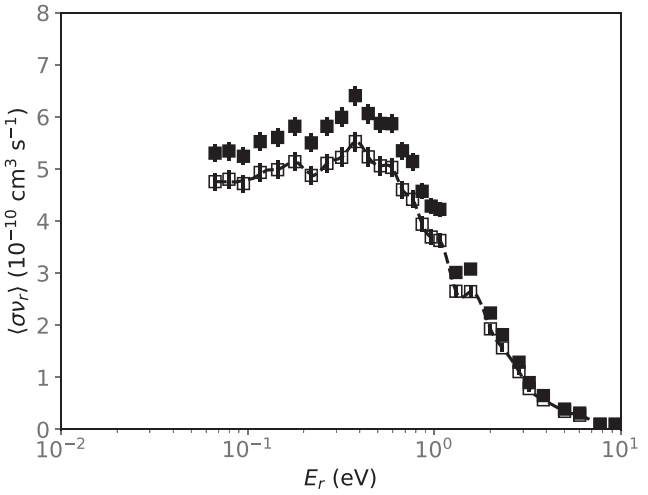

FIG. 2. The graph shows the measured data (open squares) of the rate coefficient for $HD^+ + C \rightarrow CD^+ + H$ together with a cubic spline fit (dashed line). The filled squares show the data for the same channel after correction for the contributions at higher relative energies (see main text for details).

in Sec. IV of Ref. [31], the distribution of the relative collision energy has a component at higher collision energies that is caused by collisions inside the 6° deflectors that merge and demerge the beams and, to a smaller extent, by the focusing quadrupole doublets inside the straight CSR section (acting only on the stored ion beam).

Figure 1 shows exemplary distributions of the relative collision energies for velocity-matched beams and for detuned beams, where the kinetic energy of the neutral beam is shifted by 0.5 keV, 1 keV, and 2 keV with respect to the matched-velocity setting. In order to depict the contribution towards higher collision energies, we chose a double-logarithmic representation in which also the size of the bins scales logarithmically with energy (note that this representation over-emphasizes the contributions at higher energies). The events at energies greater than 10 eV stem almost exclusively from collisions inside the 6° deflectors, which account for about 6.6% of all collisions. However, since the rate coefficients for our experiments typically tend toward zero at such high collision energies, these events will have very little impact on the overall shape of our data, but they influence the absolute calibration of our measurements. Inside the focusing quadrupoles of the CSR the stored particles experience a deflection dependent on the displacement of the ions from their central orbit. A fraction of about ∼10% of all events takes place inside the quadrupoles and distorts the distribution of the relative collision energies (appearing as a shoulder exceeding relative collision energies of 1 eV for matched velocities in Fig. 1).

In order to correct for the contributions at higher collision energies, we developed a simple iterative numerical procedure. We generated the distributions of the relative collision energies for every nominal neutral beam energy setting that was used in our experiments, utilizing G4BEAMLINE Monte Carlo simulations. These discrete distributions were normalized to the total number of events to calculate the relative probability $p(E_r')$ with which a certain collision energy E_r' will be sampled at this particular setting. The measured rate coefficients $k(E_r)$ were interpolated by a cubic spline fit (at high collision energies the rate coefficients approach zero), yielding smooth functions $k_S(E_r)$. For the correction, we start with the data point measured at the highest collision energy and go step by step towards smaller collision energies. The corrected rate coefficient k_{corr} is determined by

$$k_{\mathrm{corr}}(E_r) = \left(k(E_r) - \sum_{E_r'>E_r^{\mathrm{min}}} k_S(E_r')\, p(E_r')\right) \Bigg/ \left(1 - \sum_{E_r'>E_r^{\mathrm{min}}} p(E_r')\right), \tag{5}$$

where E_r^{min} denotes the transition energy where a particular simulated collision energy distribution begins to be dominated by the unwanted events stemming from the quadrupole and merging regions. This procedure is repeated for each data point, but in each step the spline fit is recalculated, including the corrected data points, and the appropriate distribution $p(E_r')$ of the simulated collision energies for this particular setting is used.

To illustrate the effect of the correction, we show both the measured and corrected rate coefficients for the $HD^+ + C \rightarrow CD^+ + H$ channel in Fig. 2. The comparison shows that the overall shape of the rate coefficient is only minimally affected by the correction, which, in fact, could be approximated rather well by an overall scaling factor (at close inspection the correction changes the shape of the curve slightly, as the effective scaling factor becomes smaller at lower energies).

The error bars shown here and throughout this work depict only 1σ statistical uncertainties derived from the absolute number of counts in each energy bin, using Poisson statistics. The systematic uncertainties and the absolute scale of the measurements will be discussed in detail in the next section.

TABLE I. Typical experimental values for the quantities given in Eq. (4) with their corresponding uncertainties.

Source	Symbol	Value	Units	Uncertainty (%)
Count rate	S	0–10	Hz	2–25
Neutral cup calibration	γ	8.5		15
Neutral C flux (secondary electrons)	I_{e^-}	300	nA	5
Stored ion beam current	I_{HD^+}	1500	nA	14
HD^+ velocity	v_{HD^+}	1.6×10^8	cm s^{-1}	$\ll 1$
C velocity	v_C	1.6×10^8	cm s^{-1}	$\ll 1$
Overlap form factor	$\langle\Omega(z)\rangle$	0.35	cm^{-2}	25
Interaction length	L	480	cm	2
Product transmission	T_p	0.9		10
Detection efficiency	η	0.95		5
Total systematic uncertainty (excluding the count rate S)				34

C. Absolute scaling of the measured rate coefficients

For absolute rate coefficient measurements we need to determine all experimental quantities given in Eq. (4). Typical experimental values together with the respective uncertainties are given in Table I. The individual uncertainties are considered as independent and added in quadrature, amounting to a total systematic uncertainty of 34%. The largest contributions are the overlap form factor between the beams with 25% and the calibration of the neutral cup with 15%. However, by calibrating our $HD^+ + C$ experiment to previous $D_2^+ + C$ experiments [28,31], the uncertainty of the absolute scale of our measurement can be reduced.

Therefore, we carried out an additional campaign to measure the ratio of the rate coefficients for the reactions $HD^+ + C$ and for $D_2^+ + C$. Both experiments were performed during the same day, and we retained the kinetic energy for the stored ions (HD^+ and D_2^+) at 40 keV. In order to measure the rate coefficients in the same range of relative collision energies for both experiments, we scaled the initial kinetic energy of the C atom beam by a factor of 4/3 for the D_2^+ measurements. Furthermore, the molecular ions were guided through the same set of 4.5 mm apertures as the neutral beam, in order to ensure a constant emittance at injection. All ion optical elements inside the CSR remained at the same potentials. Consequently, we assume that the overlap $L\langle\Omega(z)\rangle$, the detection efficiency η and the transmission T_p of the products in the extraction beam line are unchanged between both measurements.

The C atom flux I_C and the stored ion beam currents I_{HD^+}, $I_{D_2^+}$, which are constantly monitored during the measurements, are inferred indirectly. Both detection techniques rely on calibration measurements performed routinely during a beam time.

The number of stored ions is determined by bunching the ion beam and detecting the mirror charge in a dedicated capacitive pickup electrode inside the CSR. This technique allows for an absolute measurement of the number of ions stored in the ring. However, since the ion-neutral measurements are performed with an unbunched beam, we use the number of neutral events created by the stored ions in interactions with the residual gas in the ring, which is constantly recorded during the measurements. This number is calibrated in a standard procedure to the capacitive pickup method and considered proportional to the number of ions in the ring (as long as the pressure inside the vacuum chambers does not change).

The C atom flux I_C propagating along the ion-neutral interaction section of the CSR is recorded in a neutral cup [31]. Inside the neutral cup the C atoms impinge on a copper surface, and secondary electrons are emitted. The resulting current I_{e^-} is proportional to the neutral C atom flux, e.g., $I_C = I_{e^-}/\gamma$. The proportionality factor γ represents the average yield of secondary electrons per neutral impact. This yield depends on the species, the charge state and velocity of the impinging particle, as well as the target material and its surface condition. The condition of the copper surface in terms of its oxide layer and adsorbed water vapor can change over time, which will also result in a change in the γ conversion factor during a beam-time campaign. These fluctuations are taken into account by the uncertainty given in Table I.

Since we link the experiments on $HD^+ + C$ and $D_2^+ + C$, many of the larger uncertainties in Table I are no longer relevant. One additional parameter that becomes relevant, however, is the relative change in the γ factor between a carbon beam at a kinetic energy of 120 keV and at 160 keV. For this purpose, we determined the γ factors for C^+, C, C^- at kinetic energies of 120 keV and 160 keV in a separate measurement. The energy dependence $\gamma(160\,\text{keV})/\gamma(120\,\text{keV})$ for all three charge states agreed well within the uncertainty.

Figure 3 compares the measured rate coefficients as a function of the collision energy for the reactions $HD^+ + C$ forming CH^+ and $D_2^+ + C$ forming CD^+, recorded in measurements carried out during the same day. Our experimental result on the rate coefficient of $D_2^+ + C$ forming $CD^+ + D$ is scaled to the previous single-pass experiment by Hillenbrand *et al.* [28], using the parametrization curve given in Schuette and Gentry [25]. Note that this curve had to be scaled by a factor 0.796 in order to match the more recent data of Hillenbrand *et al.* (see original publication for details [28]). This small difference in the absolute scaling can probably be attributed to the fact that the data of Schuette and Gentry were taken with neutral carbon atoms produced in a charge exchange process, where the production of carbon atoms in excited states can not be ruled out. We then proceed to fit the same curve to our data for the CH^+ channel in the reaction of HD^+ and C, and we infer a scaling factor of 1.66 ± 0.06 between the two fits.

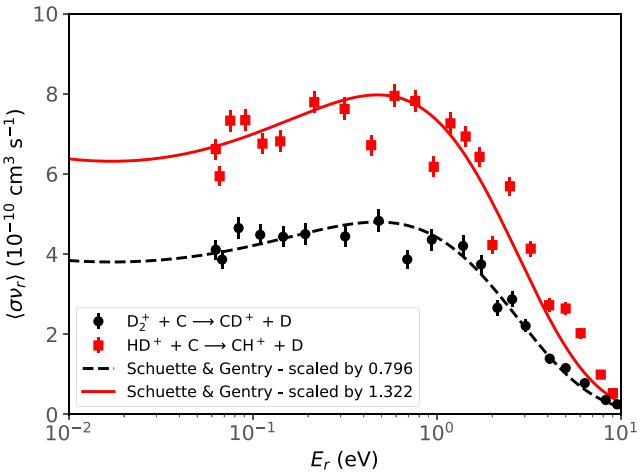

FIG. 3. Measured merged-beams rate coefficients for the reaction $D_2^+ + C \rightarrow CD^+ + D$ (represented by the black dots) and for the reaction $HD^+ + C \rightarrow CH^+ + D$ (indicated by the red squares) as a function of their relative collision energy. The (dashed) black and (solid) red lines, respectively, represent the scaled previous single-pass experiment on $D_2^+ + C \rightarrow CD^+ + D$ by Schuette and Gentry [25]. The scaling factors are given in the inset, they have been derived by a least-squares fit.

Using this value and the same fit function we can calibrate the absolute scale of our $HD^+ + C$ measurements to the previous benchmark experiment. The new uncertainties for the absolute scale are given in Table II, resulting in a reduction of the total systematic uncertainty to 19%.

III. REACTIONS OF HD^+ WITH C

A. Quasiclassical trajectory calculations

The interaction between H_2^+ and C in C_s symmetry generates six electronic states of doublet and quartet spin multiplicity. In a previous study [28] of the $H_2^+ + C \rightarrow CH^+ + H$ reaction, a detailed analysis of the CH_2^+ system in the reactant and product channels led us to hypothesize that the reaction proceeds mainly through the first two $1^4A'$ and $1^4A''$ quartet states of CH_2^+. Both states correlate adiabatically the reactants to the $CH^+(^3\Pi) + H$ products, with an exoergicity of 2.6 eV, and correspond to attractive long-range interactions between the reactants [25]. By contrast, the third quartet state is repulsive at long range and correlates to the $CH(^4\Sigma^-) + H^+$ products. The three doublet states, leading to form the $CH^+(^1\Pi) + H$ and $CH(^2\Pi) + H^+$ products, exhibit potential energy barriers at short range [41] out of collinear geometry of the reactants. Moreover, multiple nonadiabatic transitions between the doublet states along the path to $CH^+(^1\Pi) + H$ are expected to reduce further their contribution to CH^+ formation [25,28,41]. We thus chose to focus on the $1^4A'$ and $1^4A''$ quartet states to treat the dynamics of the $HD^+ + C$ reaction.

Potential energy surfaces (PES) for the $1^4A'$ and $1^4A''$ quartet states have recently been developed by some of us [42]. They are based on *ab initio* energies obtained from multireference configuration interaction [43,44] calculations, with Davidson correction [45], and using aug-cc-pVQZ basis sets [46,47] for carbon and hydrogen. Analytical representations of the two global PESs were built up by means of the reproducing kernel Hilbert space method [48]. In the reactant channel, at large separation between H_2^+ and C, each PES is matched with an analytical potential describing the two main contributions to long-range (LR) interactions, namely the charge-quadrupole and charge-induced dipole interactions. Since these LR interactions involve H_2^+ only as a point charge, the associated LR potentials are isotropic and independent of the bond length of H_2^+. Discarding the spin-orbit interactions, the states correlating with $H_2^+ + C$ give rise to two distinct LR potentials, each of them being characterized by a specific value of $|M_L|$, where $M_L = 0, \pm 1$ is the projection of the orbital angular momentum L of $C(^3P)$ on the ion-atom axis. For both the $1^4A'$ and $1^4A''$ states, which form a $^4\Pi$ state in $C_{\infty v}$ symmetry and thus correlate with the $M_L = \pm 1$ state of $C(^3P)$, the LR potential writes [49]

$$V_{\mathrm{LR}}(R) = \frac{1}{R^3} q\, \Theta_C^{|M_L|=1} - \frac{1}{R^4} \frac{q^2}{2} \alpha_C^{|M_L|=1}, \tag{6}$$

where R is the distance between C and the center of mass of H_2^+, q is the charge of H_2^+, $\Theta_C^{|M_L|=1} = -0.705$ a.u. and $\alpha_C^{|M_L|=1} = 12.41$ a.u. are, respectively, the permanent quadrupole moment [50] and the static dipole polarizability [51] corresponding to the $M_L = \pm 1$ state of $C(^3P)$. It is worth noting that the value tabulated in Ref. [50] for the quadrupole moment of carbon $C(^3P)$ corresponds to $\Theta_C^{M_L=0} = \langle M_L = 0 | \hat{\Theta}_{zz} | M_L = 0 \rangle = -2\Theta_C^{|M_L|=1}$. Also, the quadrupole moment operator $\hat{\Theta}_{zz}$ defined in Ref. [50] differs by a factor of two from the one of Ref. [49]. Accordingly, the values of $\Theta_C^{|M_L|}$ in Refs. [49,50] differ by a factor of two.

TABLE II. Typical experimental values and uncertainties for the relevant quantities needed for absolute measurements after calibration to the $D_2^+ + C$ data of Hillenbrand *et al.* [28].

Source	Symbol	Value	Units	Uncertainty (%)
Count rate	S	0–10	Hz	2-25
Neutral cup calibration	$\gamma(160\,\mathrm{keV})/\gamma(120\,\mathrm{keV})$	1.14		3
Neutral C flux (secondary electrons)	I_{e^-}	300	nA	5
Ratio of stored ion beam currents	$I_{HD^+}/I_{D_2^+}$	1.3		10
Fit for the calibration ratio	$f(HD^+)/f(D_2^+)$	1.66		4
Systematic uncertainty Hillenbrand *et al.* [28]				15
Total systematic uncertainty (excluding the count rate S)				19

The two $1^4A'$ and $1^4A''$ global PESs are barrierless. They both correlate the $H_2^+ + C$ reactants with the $CH^+(^3\Pi) + H$ products, and share the same attractive LR potential in the reactant channel, as well as the same $^4\Pi$ PES for collinear approach of the reactants. The two PESs differ most notably by the presence of a deep potential energy well on the $1^4A''$ PES that lies 4.9 eV below the $H_2^+ + C$ dissociation limit and corresponds to a bent CH_2^+ equilibrium structure of C_{2v} symmetry [52]. As a consequence, the $1^4A''$ PES favors the perpendicular configuration of the reactants when they get close to each other, while the $1^4A'$ PES favors the collinear one.

The $1^4A'$ and $1^4A''$ PESs were employed to perform quasiclassical trajectory (QCT) calculations of the reaction cross sections associated with the $CH^+ + D$ and $CD^+ + H$ product channels of the $HD^+ + C$ reaction. The QCT program, originally developed by Halvick and Rayez [53], is based on a standard Monte Carlo sampling of the initial conditions [54]. The calculations were carried out for 36 values of the collision energy E_r ranging from 0.01–10 eV. For comparison with the merged beams measurements, the HD^+ molecular ion was initially set in its ground vibrational state ($v = 0, J$) with rotational states J sampled according to a thermal distribution at 150 K (this temperature is motivated by models of the evolution of the internal excitation of the stored ions, see next section). The initial distance R between C and HD^+ was varied between 20 Å and 70 Å such that the interaction energy represents less than 0.1% of the collision energy. Each trajectory was integrated in time using a Runge-Kutta algorithm, with a time step of 0.01 fs, until the translational energy of the products varied by less than 10^{-7} eV. For all trajectories the total energy was found to be conserved within 0.006%. Due to a significant decrease of the reaction probabilities at high collision energy, different batches of trajectories were run depending on the energy range: 5×10^4 trajectories for $E_r < 2$ eV, 1×10^5 for $2 \leqslant E_r < 5$ eV, and 2×10^5 for $E_r \geqslant 5$ eV. This ensured statistical deviations of less than 1% for all QCT cross section values.

For the present study, we had also to pay particular attention to the formation of CH^+ and CD^+ quasibound molecules in the product channels. Indeed, the $C^+ + H + D$ dissociation limit lies only 0.46 eV above the reactants (reduced to 0.34 eV when accounting for the zero-point energy of HD^+), and the dissociative charge transfer (DCT) reaction,

$$HD^+ + C \rightarrow C^+ + H + D \tag{7}$$

becomes a major competing process for collision energies higher than the DCT energy threshold. Furthermore, above this energy threshold, the CH^+/CD^+ molecules can be produced with internal energies greater than their dissociation energy, and still be bound by the centrifugal energy barrier induced by their rotational angular momentum. This leads to quasibound molecules whose finite lifetime depends on the probability of tunneling through the centrifugal barrier [55]. In the present experiment, the flight time from the interaction region to the particle detector is about 6 μs. Hence, quasibound molecules having lifetimes longer than this value should contribute to the measured reaction cross sections. In the QCT calculations, the quasibound CH^+/CD^+ product molecules were identified as follows. First, we assign each product channel of reactions (1a), (1b), and (7) by imposing different conditions on the internuclear distances at the end of each trajectory. Then, we discriminate the bound and quasibound species produced by reactions (1a) and (1b) by comparing the internal energies of the CH^+/CD^+ molecules to their dissociation energy.

The influence of quasibound product molecules on the reaction cross sections was evaluated by considering two limiting cases in the QCT calculations. In the first case, we assume that all of the CH^+/CD^+ bound and quasibound molecules contribute to reactions (1a)/(1b). In the second case, we assume that only the bound species contribute to reactions (1a)/(1b). The QCT results labeled hereafter "including" and "excluding" quasibound states refer to these first and second limiting cases, respectively. Whatever the case considered, the QCT cross sections computed at each collision energy E_r from the $1^4A'$ and $1^4A''$ PESs were finally averaged as

$$\sigma_\alpha(E_r) = p_\alpha^{A'}\sigma_\alpha^{A'}(E_r) + p_\alpha^{A''}\sigma_\alpha^{A''}(E_r), \tag{8}$$

where $\alpha = CH^+/CD^+$ for reactions (1a)/(1b), respectively, and $p_\alpha^{A'} = p_\alpha^{A''} = 4/18$ is the probability for the $HD^+ + C$ collision to initiate on one of the two reactive PESs [28]. In C_s symmetry, this probability stems from the spin degeneracy of each electronic state involved in the collision: among the three doublet and three quartet electronic states that correlate with the reactants (amounting to 18 states, which are degenerate in the asymptotic limit), only the $1^4A'$ and $1^4A''$ quartet states are assumed to lead to the reaction products. The rate coefficients associated with each reaction channel were determined from the QCT cross sections as:

$$k_\alpha(E_r) = \sigma_\alpha(E_r)v_r, \tag{9}$$

where v_r is the relative velocity of the $HD^+ + C$ reactants.

B. Internal excitation of the stored HD^+ ions

After injection into the cryogenic vacuum of the CSR the HD^+ ions will begin to cool by spontaneous emission of radiation. The initial excitation of molecular hydrogen ions, coming from standard electron impact ion sources, has been studied extensively [58]. Typically, the majority of the molecules of the neutral parent gas are assumed to occupy the vibrational ground state, such that the vibrational distribution of the ionized molecules is given by the matrix element for ground-state electron impact ionization [28]. However, for the present experiment the ion beam is stored long enough for complete relaxation to the vibrational ground state. In fact, directly applicable experimental data exist, as the vibrational cooling of HD^+ extracted from a discharge ion source was studied *in situ* at the Test Storage Ring. Using foil-induced Coulomb explosion imaging, the vibrational wave function of the stored ion sample was monitored as a function of storage time, and cooling curves for the individual vibrational states [Fig. 4(a)] were derived [56]. It was found that after 300 ms of storage, more than 96% of the ions occupy the vibrational ground state. With a lifetime of ~60 ms the remaining population in the $v = 1$ state will also decay quickly, and we can

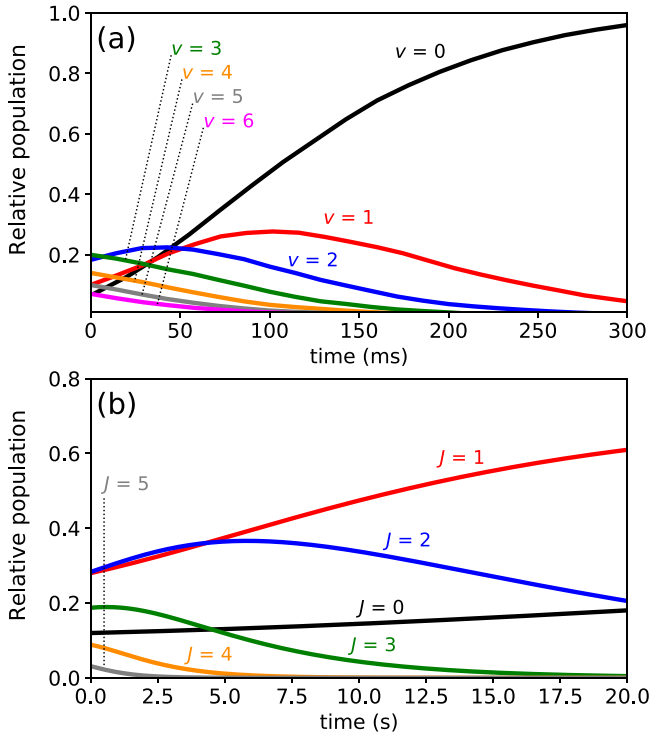

FIG. 4. Evolution of the (a) vibrational and (b) rotational states of HD^+ during storage inside the CSR. The vibrational cooling has been measured at the TSR previously [56]. The initial rotational distribution is modeled for a neutral gas temperature of 500 K inside the ion source, assuming that electron impact does not change the angular momentum of the molecules. The time evolution of the population is based on published Einstein coefficients and level energies for HD^+ [57].

safely assume vibrational cooling to be complete after 0.5 s of storage.

A model of the evolution of the rotational populations inside the CSR is shown in Fig. 4(b). As in previous work [28], our calculations are based on two common assumptions: (i) the temperature of the neutral gas inside of the ion source is estimated to be 500 K, (ii) electron impact ionization does not change the angular momentum of the molecules. Since the rotational constants of neutral HD ($B_e = 44.7\ \mathrm{cm}^{-1}$ [59]) and HD^+ ($B_e = 21.9\ \mathrm{cm}^{-1}$ [57]) differ substantially, this results in an initial HD^+ rotational temperature of approximately ~245 K upon injection into the CSR. The evolution of the rotational states inside the storage ring can be predicted in a straightforward manner by solving the ordinary differential equations that couple the rotational states by radiative transitions, using published Einstein coefficients for the transition probabilities [57]. The results of the calculation are shown in Fig. 4(b) and in Table III. As we did not observe any change in the signal after 0.5 s of storage, we have averaged the populations for the stored ions from 0.5–20 s, which essentially spans the entire storage time window that was used for the present experiment, excluding the initial period required for vibrational cooling. Comparison with a thermal HD^+ distribution at 150 K gives reasonable agreement. We have used this estimated temperature as an input for the QCT calculations presented in Sec. III A.

TABLE III. Estimated relative populations of the seven lowest rotational states of HD^+. The first column gives the angular momentum quantum number J, the second column gives the level energy, the third column gives the initial populations based on electron impact ionization at 500 K (see main text for details), the fourth column gives the average populations for storage times from 0.5–20 s, and the final column gives the populations for a thermal ensemble at 150 K for comparison.

J	Energy (cm^{-1})	Initial population	Average 0.5–20 s	Thermal 150 K
0	0.0	0.12	0.15	0.20
1	43.8	0.29	0.47	0.39
2	131.1	0.28	0.31	0.28
3	261.5	0.18	0.07	0.11
4	434.1	0.08	0.01	0.03
5	647.9	0.03	0.00	0.00
6	901.8	0.01	0.00	0.00

C. Subtracting the contribution from H_3^+ beam contamination

While we produce the HD^+ ions using HD gas inside a discharge ion source, we found that we can not avoid small contaminations by triatomic hydrogen. After extracting and accelerating the ions from the source, we use a 90° dipole magnet to filter the desired mass-to-charge ratio. Scanning the mass-to-charge ratio between 1 and 6 atomic units allowed us to quantify the fraction of triatomic ions to diatomic ions and thus to estimate the fraction of H_3^+ ions in the main HD^+ beam to be ~4%. To correct for this beam impurity, it is not sufficient to introduce a calibration factor for the number of stored ions inside the CSR, since the H_3^+ ions will react with the neutral C atoms [reactions (2a) and (2b)] and the two possible reaction products have the same mass as the products involving HD^+ ions [reactions (1a) and (1b)].

In order to be able to subtract the contribution of this contamination, we conducted an independent measurement of the rate coefficients of H_3^+ reacting with C, by using H_2 gas in the ion source and increasing the pressure to favor the formation of triatomic hydrogen. For the correction, the rate coefficients for reactions (2a) and (2b) are fitted first, in order to interpolate the data points (see Fig. 5). For reaction (2a) we apply the empirical fit function derived by O'Connor *et al.* for previous measurements of this reaction (Eq. (28) in Ref. [26]), represented by a black line in Fig. 5(a). Since we spent only a comparatively short time on the H_3^+ measurement, our data points display a larger fluctuation. For reaction (2b) we applied the fit function used in de Ruette *et al.* (Eq. (12) in Ref. [27]), plotted as a black line in Fig. 5(b).

Using these interpolations and assuming a 4% H_3^+ beam contamination, we can subtract its contribution from the measured rate coefficients for $HD^+ + C$ forming CH^+ and CD^+, respectively. Since the contamination impacts the measured number of stored HD^+ ions, the result has to be scaled up by that fraction.

The corrected rate coefficients are indicated by the red and blue solid symbols in Fig. 5. Note that the overall correction leads to a slight decrease in the rate coefficient for the CH^+ channel [as the subtracted rate coefficient for reaction (2a)

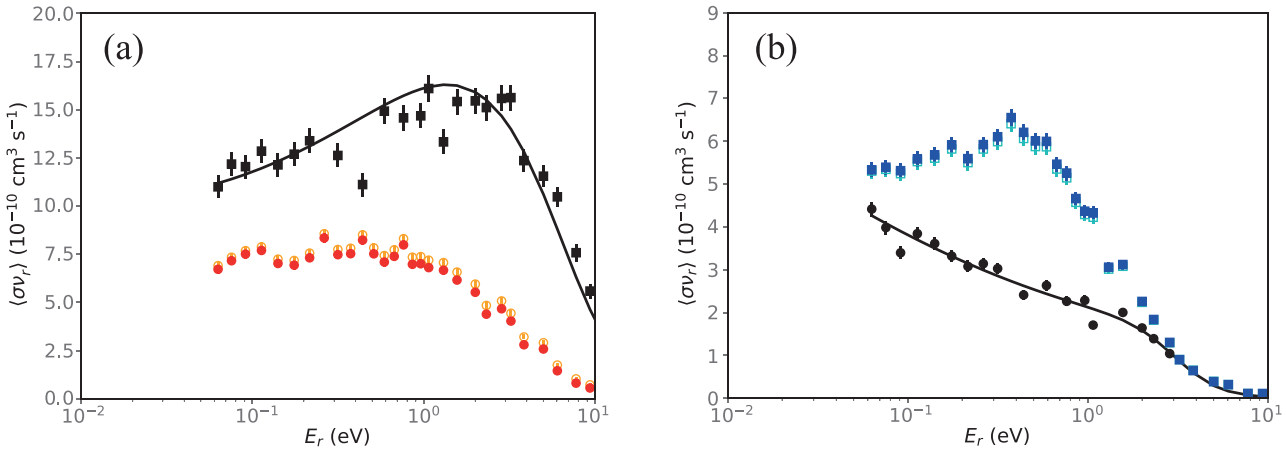

FIG. 5. (a) The open red dots indicate the measured rate coefficient for the reaction $HD^+ + C$ forming CH^+ [reaction (1a)]. The black squares show the measured rate coefficient for $H_3^+ + C$ forming CH^+ [reaction (2a)] with a fit to the data (black line). The red solid dots show the rate coefficient for reaction (1a) after the 4% contribution from reaction (2a) has been subtracted and the rate coefficient has been scaled by the appropriate factor (see main text for details). (b) The open blue squares indicate the measured rate coefficient for the reaction $HD^+ + C$ forming CD^+ [reaction (1b)]. The black dots show the measured rate coefficient for $H_3^+ + C$ forming CH_2^+ [reaction (2b)] with a fit to the data (black line). The blue open squares show the rate coefficient for reaction (1b) after the 4% contribution from reaction (2b) has been subtracted and the rate coefficient has been scaled by the appropriate factor.

is higher compared to reaction (1a)], while the corrected rate coefficient for the CD^+ channel is increased [as the as subtracted rate coefficient for reaction (2b) is lower than for reaction (1b)].

The main purpose of the $H_3^+ + C$ measurements for the present work was to quantify the effect of the contamination on the $HD^+ + C$ data. Therefore, we used the same storage time window and settings to obtain a fair correction.

However, the reaction of H_3^+ with C is a very interesting process in its own right. In fact, it is often assumed that this reaction introduces carbon into the interstellar chemistry network, and therefore is responsible for the onset of organic chemistry in the gas phase of interstellar clouds. While the rotational distribution sampled for the present experiment is not well defined, the fact that the H_3^+ ions have time to cool vibrationally inside the CSR already marks a major advantage over single-pass experiments. Hence, it is interesting to compare the absolute magnitude of our (vibrationally cold) H_3^+ rate coefficients to previous (hot) measurements and capture theories. This comparison will be discussed in later sections.

D. Results for reactive $HD^+ + C$ collisions

We measured the rate coefficients of reactions (1a) and (1b) for storage times of up to 20 s. As described above, we expect the vibrational cooling to be complete after 0.5 s [Fig. 4(a)], while the rotational distribution at these storage times is still evolving slowly among the lowest rotational states [Fig. 4(b)]. In both reaction channels the data did not reveal any significant changes after 0.5 s of storage. Figure 6 shows the merged beams rate coefficients for both reaction channels divided into ∼5 s long storage time intervals (while excluding the first 0.5 s). The plots show that there are no statistically relevant trends visible in the data after vibrational cooling is complete. From here on we will sum up all storage

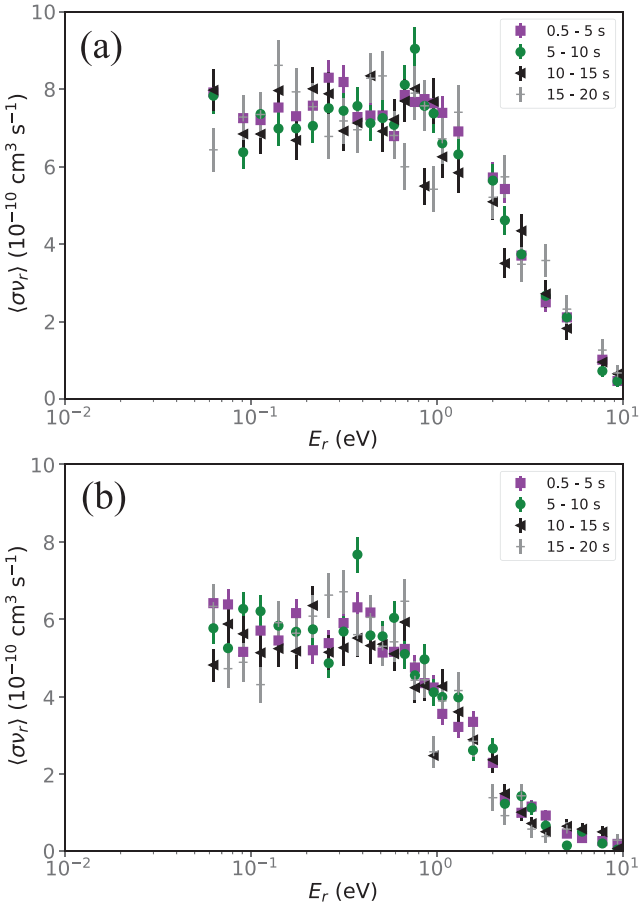

FIG. 6. Merged beams rate coefficient for (a) $HD^+ + C \rightarrow CH^+ + D$ and (b) $HD^+ + C \rightarrow CD^+ + H$ for different storage time intervals, as given in the insets. These plots illustrate that no statistically relevant changes can be discerned after 0.5 s of storage.

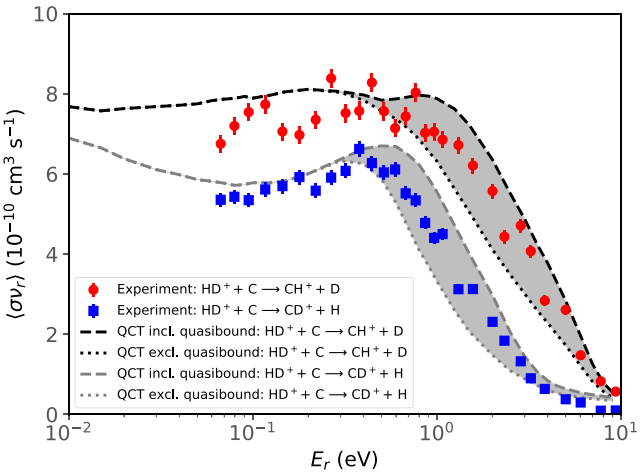

FIG. 7. Merged beams rate coefficients for $HD^+ + C \rightarrow CH^+ + D$ (red circles) and $HD^+ + C \rightarrow CD^+ + H$ (blue squares) as a function of the relative collision energy. Storage times from 0.5–20 s were included. The dashed lines present QCT calculations (see Sec. III A), where the shaded areas represent the difference between calculations including or excluding all quasibound product molecules (see main text for details).

times after 0.5 s as vibrationally cold data, to improve the total statistics.

Figure 7 shows the rate coefficients for both reaction channels in a storage time interval from 0.5–20 s. The rate coefficients have been corrected for the H_3^+ contamination (Sec. III C) and the simulated contributions from higher energies in the quadrupole and merging sections (Sec. II B). After these corrective steps, the plotted data represent merged beams rate coefficients $\langle \sigma v_r \rangle$ that are valid for each relative detuning energy $E_r = \frac{1}{2}\mu v_r^2$, where μ denotes the reduced mass. The error bars in the graph represent 1σ uncertainties derived only from the counting statistics at each energy bin, assuming Poisson statistics ($\delta N = \sqrt{N}$). We estimate an additional total uncertainty of ~20% for the absolute scale of the rate coefficients (Sec. II C), as our data have been scaled to the $D_2^+ + C$ rate coefficient measurements of Ref. [28]. The lowest energy that can be sampled by the experiment in its current form is on the order of 60 meV, mainly due to the angular spread of the two beams. Also shown in the plot is the outcome of the QCT calculations for both channels, which match the measured rate coefficients very well. Almost across the entire energy range, the agreement between experiment and theory is excellent, indicating that the $1^4A'$ and $1^4A''$ states indeed provide the main contribution to reactions (1a) and (1b). The experimental values lie between the two limits of the QCT calculations at high energies, where either all molecules in quasibound states are assumed to contribute to the signal, or none of the molecules in quasibound states contribute (see Sec. III A). This implies that a fraction of the quasibound molecules live long enough to make it to the particle detector.

The impact of vibrational excitation on the rate coefficients is more difficult to assess, as it can only be observed during the first few hundred milliseconds of storage. Quantitative analysis of the rates at these short times is rather challenging. First, we can not take data in the first 50 ms, as the stabilization of the orbit of the stored ions after injection takes a while. At these short storage times the beam overlap might still change slightly. Furthermore, for the determination of the number of stored ions, we rely on neutralization events of the stored beam with residual gas ions. However, we found that for vibrationally excited ions the cross section for neutralization appears increased. This is manifested in a fast decay component in the neutralization signal visible during the first 200 ms. This component constitutes about 20% of the total signal, and we believe that it does not indicate an actual excess of ions, but a change in the neutralization efficiency during the vibrational cooling. Figure 8 provides a qualitative representation of the change of the rate coefficients for both reaction channels at very short storage times.

To cope with the rather poor statistics of individual data points at these short storage time intervals, we decided to sum up the rate coefficient into a single curve and provide uncertainty bands for three storage time intervals, taking into account the uncertainty in the absolute number of ions caused by the excess neutralization signal at short storage times in the width of the shaded areas. The purpose of this illustration is to show that, even including the additional uncertainties in the calibration procedure, a clear trend toward lower rates with decreasing storage time (and thus increasing vibrational excitation) is found. This trend is consistent with the low rate coefficients measured for the vibrationally excited H_2^+ and D_2^+ ions in previous single-pass experiments [28].

IV. REACTIONS OF H_3^+ WITH C

The triatomic hydrogen ion H_3^+ is one of the most important species for the chemistry of interstellar space. As an active proton donor, it reacts with many heavier species, and thus H_3^+ initiates an active ion-neutral chemistry network in molecular environments. The reaction between H_3^+ and C atoms is particularly interesting, as it introduces carbon into the network by forming CH^+ and CH_2^+, and thereby it enables the formation of more complex organic species.

In the present work, the H_3^+ data were mainly taken with the intent to subtract the background caused by $H_3^+ + C$ reactions from our product channels. The reason why we did not investigate the reactions with triatomic hydrogen ions in more detail in the present study lies in the complicated radiative cooling behavior of H_3^+ [60,61]. We have come to the conclusion that in order to perform experiments with H_3^+ with proper knowledge of the population of internal states, it would be preferable to develop a spectroscopic method to monitor individual states. Such efforts are currently underway [62], but not yet functional.

However, the data presented in the previous section also revealed that vibrational excitation can have a major influence on the rate coefficient, while the changing rotational excitation did not affect the rate coefficients. Therefore, our vibrationally cold H_3^+ data already represent a major improvement compared to previous single-pass experiments with highly excited vibrational states, and we decided to present them here as an intermediate status report, until rotationally state-resolved measurements are within our reach.

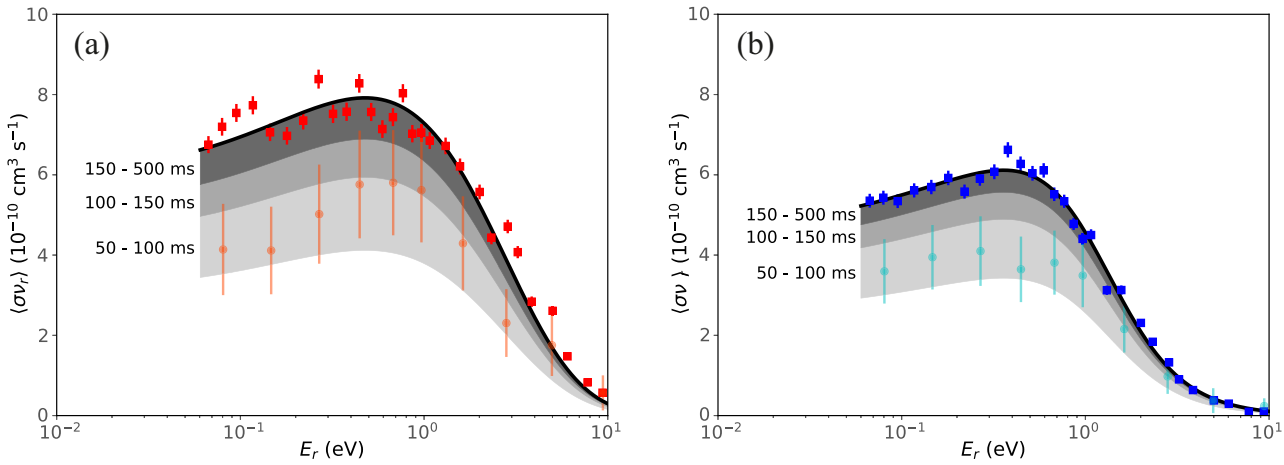

FIG. 8. Merged beams rate coefficients for (a) $HD^+ + C \rightarrow CH^+ + D$ and (b) $HD^+ + C \rightarrow CD^+ + H$ as a function of the relative collision energy. The solid squares represent the vibrationally cold data, while the shaded areas give a coarse representation of the development of the rate coefficient at very short storage time intervals, when vibrational cooling is not complete yet. The width of the shaded areas takes into account uncertainties of the normalization procedure at short storage times (see main text for details). The solid round symbols in light red (a) and light blue (b) represent exemplary data for the shortest storage time interval from 50–100 ms.

A. Internal excitation of the stored H_3^+ ions

The vibrational and rotational cooling of H_3^+ has been studied experimentally at the room-temperature Test Storage Ring [60], and extensive calculations on the radiative cooling of triatomic hydrogen have been carried out [61]. Owing to its equilateral symmetry, H_3^+ hosts both comparatively long-lived vibrational states, as well as metastable rotational levels. The initial rotational temperature observed using beams extracted from standard ion sources during the first milliseconds of storage was found to be more than 3000 K [60]. In fact, it is believed that about 2/3 of the 1.7 eV exothermicity of the classic formation reaction of triatomic hydrogen

$$H_2^+ + H_2 \rightarrow H_3^+ + H \tag{10}$$

will end up in internal excitation [63]. These excitations can partly be mitigated by subsequent collisions in the ion source, as demonstrated by more recent work on the $D + H_3^+$ atom exchange reaction, where internal temperatures on the order of 1200 K for carefully chosen pressure conditions were found [64,65]. On the other hand, H_3^+ couples only weakly to the ambient radiation field, and therefore we can assume that the cooling inside the cryogenic vacuum of the CSR follows the same initial pattern as cooling in a room temperature environment.

The most long-lived vibrational states of H_3^+ feature the symmetric breathing mode of the molecule, where the size of the molecule changes, while the triangular symmetry remains intact. The Coulomb explosion imaging experiments at TSR revealed that all vibrational states, apart from the lowest breathing mode level ($\nu_1 = 1$), decay within the first 0.5 s of storage [60]. Furthermore, the average lifetime of this breathing mode state of $\tau = 1.18$ s [66] was found to be decreased considerably due to the coupling to highly excited rotational states during the TSR experiments [60]. More quantitatively, less than 5% of the total population remained in the $\nu_1 = 1$ state at 0.5 s of storage, and after 2 s the vibrational cooling was complete (see Fig. 6 in Ref. [60]). For consistency, we will average the H_3^+ rate coefficient data over the same interval from 0.5–20 s as the HD^+ data, and we will assume that vibrational excitation does not play a significant role at these storage times any more.

The rotational cooling of H_3^+ is more complex. The lifetime of rotational states depends not only on the angular momentum number J, but, crucially, on the projection of the rotational angular momentum onto the molecular axis, represented by quantum number $K \leqslant J$ (for H_3^+ nomenclature and quantum numbers see Ref. [67]). For K approaching J, H_3^+ rotational states will become metastable, to the point that some of them have no obvious decay mechanism anymore, and for all practical intents and purposes can be considered stable with respect to radiative decay. This means that the rotational excitation of H_3^+ will cool significantly (states with low K will decay) within the first 20 s of storage, however, very highly excited states will remain populated and population will feed into these metastable states [61].

For the present study, we have to assume that the rotational excitation of H_3^+ during the first 20 s of storage is still rather high, and at the same time rapidly evolving, while the rotational distribution is not well defined. This complex cooling behavior is the main reason why we spent only limited measurement time on the $H_3^+ + C$ reaction, as the definition of rotational state populations in the present experiment is rather poor, and the implementation of a cold ion source and state-selective diagnostics are foreseen for future studies of this important ion.

B. Results of the rate coefficient measurements for reactive $H_3^+ + C$ collisions

Figure 9 shows the merged beams rate coefficients for the two reaction channels $H_3^+ + C \rightarrow CH^+ + H_2$ and $H_3^+ + C \rightarrow CH_2^+ + H$ individually. In both cases the absolute scale of the rate coefficients was normalized to the $D_2^+ + C$ calibration measurement, and the data have been corrected for the contributions at higher collision energies, caused by the

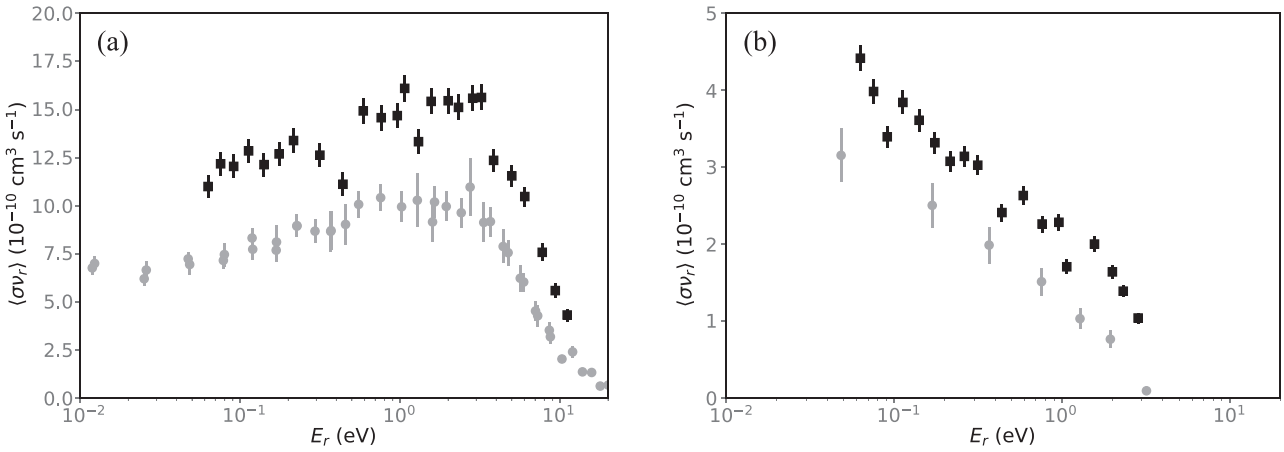

FIG. 9. Merged beams rate coefficients for (a) $H_3^+ + C \rightarrow CH^+ + H_2$ and (b) $H_3^+ + C \rightarrow CH_2^+ + H$ as a function of the relative collision energy. The solid black squares represent the present measurements for vibrationally cold H_3^+ (storage times >0.5 s), the gray dots represent the previous data of O'Connor *et al.* [26], obtained with vibrationally excited H_3^+ ions.

merging and focusing of the beams (see Sec. II B). The measurements are compared to the previous single-pass experiment of O'Connor *et al.* [26].

Despite the comparatively short time spent on this measurement, the trend of the rate coefficients agrees reasonably well with the previous data. However, the present measurements reveal an increase in both rates on the order of ∼50%. As outlined in the previous section, we expect the H_3^+ ions in the present experiment to be in their vibrational ground state, while the rotational distribution is poorly defined, and metastable states with energies as high as 1 eV may still be present.

Previous theoretical studies of the $H_3^+ + C \rightarrow CH^+ + H_2$ reaction by Talbi *et al.* and Bettens and Collins resulted in room temperature rate coefficients of 2.3×10^{-9} cm^{-3} s^{-1} [68] and 1.3×10^{-9} cm^{-3} s^{-1} [69,70], respectively. However, while the CH_2^+ formation channel was not even considered in the study of Talbi *at al.* [68], a very low rate coefficient of 1.2×10^{-11} cm^{-3} s^{-1} was predicted by Bettens and Collins [69,70]. Our measurements for the latter channel result in a rate coefficient at low collision energies that is about ∼40 times higher than these theoretical predictions, supporting the previous experimental finding of O'Connor *et al.* [26] that the CH_2^+ formation is much faster than previously assumed, and should be included in astrophysical models.

V. COMPARISON TO CAPTURE MODELS AND ASTROCHEMICAL IMPLICATIONS

Many of the ion-neutral reactions used in current databases and models have not been measured in the laboratory, and the majority of the rate coefficients in the chemical networks relies on educated guesses based on classical capture models. Therefore, it is interesting to assess the validity of these capture models for the two reaction systems studied here.

The rate coefficients measured for the $HD^+/H_2^+/D_2^+ + C$ reaction (forming CH^+ and CD^+) and the $H_3^+ + C$ reaction (forming CH^+ and CH_2^+) show that product formation operates rapidly down to collision energies of a few meV [26,28]. The absence of activation energy provides evidence that these reactions are exoergic and proceed without potential energy barrier. Under these conditions, the rate of reaction depends mainly on the ability of the reactants to pass over the centrifugal barrier in the effective potential. Capture models [71–73], which assume that each collision where the reactants can overcome the centrifugal barrier leads to reaction, are thus well suited to determine upper bounds of the reaction rate coefficients. Since capture models do not provide information on the reaction products (unless additional treatments be used [71]), the rate coefficients reported hereafter correspond to the sum over all product channels of the $HD^+ + C$ and $H_3^+ + C$ reactions.

At low collision energies, the maximum of the effective potential occurs at such large ion-neutral separation that the reactions are dominated by long-range (LR) interactions. For both reactions (1) and (2), the leading terms of long-range interactions are the charge-quadrupole and charge-induced dipole interactions, which involve HD^+ or H_3^+ only as a point charge. Moreover, when the spin-orbit interactions are neglected, each reaction proceeds through two electronic states [49,68], which are degenerate at long range and correlate with the $M_L = \pm1$ state of C(^{3}P). The $HD^+ + C$ and $H_3^+ + C$ reactions are thus characterized by the same long-range potential $V_{LR}(R)$ [given in Eq. (6)], implying that the capture cross sections should be identical for the two reactions. Since the $HD^+ + C$ and $H_3^+ + C$ reactants have the same reduced mass μ, the corresponding capture rate coefficients are also identical for reactions (1) and (2).

In a classical approach of capture theory, the effective potential writes in terms of the impact parameter b as [71–73]

$$V_{\text{eff}}(R) = \frac{E_r b^2}{R^2} + V_{\text{LR}}(R), \tag{11}$$

and the capture cross section is given by $\sigma_{\text{cap}} = \pi\, b_{\text{max}}^2$, where b_{max} is the maximal value of the impact parameter leading to a reaction. The criterion for capture $E_r \geqslant V_{\text{eff}}(R)$ defines b_{max} from the orbiting condition $E_r = V_{\text{eff}}(R_c)$, where R_c is the capture distance corresponding to the maximum of the effective potential when $b = b_{\text{max}}$. Accordingly, the reaction

cross section can be expressed as

$$\sigma_{\rm cap}(E_r) = \pi\, R_c^2\left[1 - \frac{V_{\rm LR}(R_c)}{E_r}\right], \tag{12}$$

and the definition of the capture distance implies that R_c is a solution of the following equation:

$$E_r - V_{\rm LR}(R_c) = \frac{R_c}{2}\left[\frac{dV_{\rm LR}}{dR}\right]_{R=R_c}. \tag{13}$$

When the charge-quadrupole and charge-induced dipole contributions to the long-range potential $V_{\rm LR}(R)$ are accounted for [see Eq. (6)], then Eq. (13) results in a quartic polynomial equation of which the capture distance R_c is the largest positive solution. Once R_c is known, Eq. (12) yields the cross section value, and the capture rate coefficient is given by

$$k_{\rm cap}(E_r) = \sigma_{\rm cap}(E_r) v_r, \tag{14}$$

where v_r is the relative velocity of the reactants, whose value at a given collision energy is identical for reactions (1) and (2).

Due to the open-shell nature of the carbon atom C(^{3}P), the interactions between the $HD^+ + C$ or $H_3^+ + C$ reactants produce multiple PESs, among which only a fraction leads to the reaction products through barrierless pathways. In order to get realistic values of the reaction rate coefficients, the rate coefficients $k_{\rm cap}$ are thus scaled by a factor $p_{\rm el}$ corresponding to the probability to initiate the collision on the reactive PESs [71]. For $HD^+ + C$, among the three doublet and three quartet PESs arising from the reactants in C_s symmetry, only two quartet PESs are considered as reactive. Accounting for the spin degeneracy of each electronic state, this leads to $p_{\rm el} = 8/18$. Similarly, only two of the three triplet PESs that correlate with $H_3^+ + C$ in C_{2v} symmetry are assumed to be reactive [68,69], leading to $p_{\rm el} = 6/9 = 2/3$. The reaction rate coefficients reported hereafter are thus given by $k_{\rm cap} \times p_{\rm el}$, where $k_{\rm cap}$ is the capture rate coefficient obtained from Eq. (14).

It is interesting to compare the results for $k_{\rm cap} \times p_{\rm el}$ along with the predictions of the Langevin-Gioumousis-Stevenson (LGS) capture model [74], which is commonly employed for exoergic reactions between ions and neutral atoms or nonpolar neutral molecules. In the LGS model, the anisotropy of the electronic charge distribution of C(^{3}P) is ignored. Accordingly, the leading term of long-range interactions is the isotropic charge-induced dipole interaction, corresponding to $V_{\rm LR}(R) = -q^2\alpha_C/2R^4$, where $\alpha_C = 11.7$ a.u. is the mean static dipole polarizability of carbon [51]. Using this form of long-range potential in Eqs. (12)–(14) leads to the Langevin rate coefficient

$$k_{\rm cap}^{\rm LGS} = 2\pi q\left(\frac{\alpha_C}{\mu}\right)^{1/2}, \tag{15}$$

whose value of 2×10^{-9} cm^3 s^{-1} is independent of collision energy. Since the LGS model approximates the carbon atom C(^{3}P) by a closed-shell species, the rate coefficient $k_{\rm cap}^{\rm LGS}$ is not scaled by $p_{\rm el}$ for consistency with the model hypothesis.

The rate coefficients $k_{\rm cap} \times p_{\rm el}$ and $k_{\rm cap}^{\rm LGS}$ for reactions (1) and (2) are compared in Fig. 10 together with the merged-beams results, obtained by summing up the rate coefficients measured for both product channels of each reaction. This

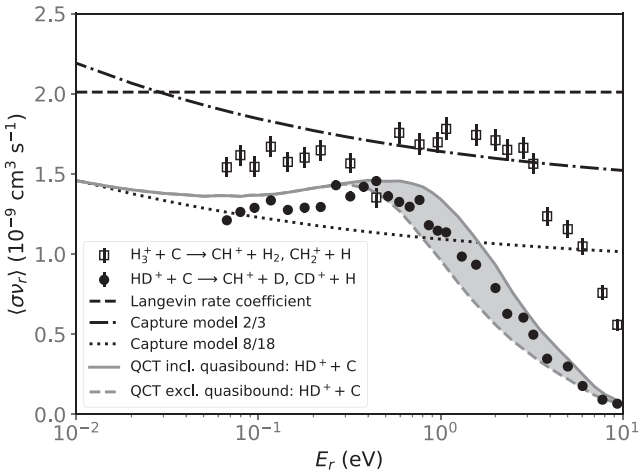

FIG. 10. Measured merged beams rate coefficients summed up for both reaction channels $H_3^+ + C \rightarrow CH^+ + H_2$ and $CH_2^+ + H$ (open symbols) and for $HD^+ + C \rightarrow CH^+ + D$ and $CD^+ + H$ (solid symbols) as a function of the relative collision energy. Full and dashed gray lines represent the total QCT rate coefficient including or excluding all quasibound product molecules. Also shown is the Langevin rate constant, based on a long-range potential taking into account the charge-induced dipole interaction (black dashed line). The dash-dotted line (termed capture model 2/3 in the inset) shows a calculation that, in addition to the induced-dipole moment, also takes into account the permanent quadrupole moment of the C(^{3}P) atom and is scaled with the relevant 2/3 fraction of reactive states for the $H_3^+ + C(^3P)$ collision system. The dotted line (capture model 8/18) shows the same calculation but scaled with the relevant fraction of 8/18 for the reactive states of the $HD^+ + C(^3P)$ collision system.

comparison is meaningful only for energies that are below the pronounced decrease of the merged-beams rate coefficients, which is due to the opening of competitive reaction channels. From Fig. 10 we can derive effective threshold energies for the main competing processes at ∼0.6 eV and ∼3 eV for the $HD^+ + C$ and $H_3^+ + C$ reactions, respectively, which may correspond with the onset of a dissociative charge transfer process in both cases [26,28]. As can be seen in Fig. 10, the LGS capture model does not allow us to discriminate between the two reactions, and, below the threshold energies mentioned before, the Langevin rate coefficient $k_{\rm cap}^{\rm LGS}$ exceeds the measurements by ∼50% and ∼25% for reaction (1) and (2), respectively. Taking into account the charge-quadrupole interaction between C(^{3}P) and the cation molecules, together with the fraction $p_{\rm el}$ of reactive states belonging to the manifold of reactant states, brings the capture rate coefficients $k_{\rm cap} \times p_{\rm el}$ in much closer agreement with the experimental data [the maximal deviation from the measurements are ∼20% and ∼12% for reaction (1) and (2), respectively]. In the particular case of the $HD^+ + C$ reaction, the excellent accord between the capture rates and the QCT values at the lowest collision energies results from the total reaction probability being close to unity in this energy range (it is found to be larger than 0.8 up to ∼0.6 eV). Increasing collision energy, the contribution of additional attractive interactions at short range, which lack in the capture model, leads to experimental and QCT rate coefficients that are increasingly larger than the $k_{\rm cap} \times p_{\rm el}$ values. For the $H_3^+ + C$ reaction, the experimental

rate coefficients are slightly smaller than the capture results at low collision energy. This discrepancy may be attributed either to a total reaction probability, which differs from unity, or to $H_3^+ + C$ interactions which are less attractive than it is assumed in the capture model. Clearly, more sophisticated calculations are needed to firmly attribute the origin of the observed deviations.

We can compare the measured rate coefficients for both reactions to the values listed in astrochemical databases to assess their implications for interstellar chemistry. The UMIST database [75] and the KIDA database [76] both list the following rate coefficients for the two reactions:

$$H_2^+ + C \rightarrow CH^+ + H,\ k = 2.4\times10^{-9}\mathrm{cm}^3\,\mathrm{s}^{-1}, \quad (16)$$

$$H_3^+ + C \rightarrow CH^+ + H_2,\ k = 2.0\times10^{-9}\mathrm{cm}^3\,\mathrm{s}^{-1}, \quad (17)$$

and in both cases it is assumed that the rate coefficients are independent of temperature between 10 and 280 K. The origins of the rate coefficients are stated as "literature search" or "estimation". The constant values suggest that the LGS capture model was used to estimate the rate coefficients. For the temperature range listed in the databases, our data from the experiment with HD^+ ions, for which we assumed a rotational distribution corresponding to 150 K, are well suited, especially since we did not see any effect of rotational cooling. For the experiment with H_3^+ ions, however, the rotational temperature is not well defined. Nevertheless, as our measurements are at least carried out with vibrationally relaxed ions, the results are still better suited than most experiments where neither rotational nor vibrational states are well defined.

Considering the $H_2^+ + C$ reaction first, our data for $HD^+ + C$ indeed indicate that the rate coefficient is essentially constant at low energies. Taking the sum of both isotopic reaction channels (as shown in Fig. 10), we measured values around $1.3\times10^{-9}\mathrm{cm}^3\,\mathrm{s}^{-1}$. Using this value and scaling it for the difference in reduced mass (assuming that there is no intermolecular isotope effect for the cross section, consistent with the findings of Hillenbrand *et al.* [30] for H_2^+ and D_2^+ reacting with C), we would expect a rate coefficient of $1.8\times10^{-9}\mathrm{cm}^3\,\mathrm{s}^{-1}$ for the reaction $H_2^+ + C \rightarrow CH^+ + H$ at low temperatures. This value is lower than the value used in the databases and should therefore be updated. However, since this reaction is less relevant for interstellar chemistry than the reaction $H_3^+ + C$, the impact on interstellar cloud models is probably very limited.

Considering the reaction $H_3^+ + C$, we find that both reaction channels combined (as plotted in Fig. 10) result in a rate coefficient of $1.6\times10^{-9}\mathrm{cm}^3\,\mathrm{s}^{-1}$ at low collision energies, which is lower than the value reported in the databases. More importantly, our data show that the rate coefficient for the CH^+ channel reaches a much lower value at low temperatures (about half of the database value), while the CH_2^+ channel continues to grow to values $>4\times10^{-10}\mathrm{cm}^3\,\mathrm{s}^{-1}$. This channel is not considered in any of the astrochemistry databases thus far, as already discussed by O'Connor *et al.* [26] in their study involving vibrationally excited H_3^+. Consequently, the change in the overall rate coefficient for the important $H_3^+ + C$ reaction and the branching between the CH^+ and CH_2^+ products should be corrected in the relevant databases.

VI. SUMMARY AND CONCLUSION

We have performed merged beams studies of reactions between stored molecular HD^+ and H_3^+ ions and ground term C atoms. The molecular ions were stored in the cryogenic vacuum of the CSR, where they had time to relax to the vibrational ground state. The rotational distribution of the stored HD^+ ions for storage times from 0.5–20 s was modeled using published transition probabilities and common assumptions on the ionization process, resulting in a distribution of rotational states with $J \leqslant 4$, which can be approximated reasonably well with a thermal ensemble of 150 K temperature. The rotational cooling of H_3^+ is much more complex, and individual rotational state occupations during the experiment are not well defined. The neutral atoms are produced by laser photodetachment of C^- anions, resulting in a ground term C (^{3}P) beam, for which we assume a thermal population of the fine structure levels.

We have measured the rate coefficients for collisions between HD^+ and C forming CH^+ and CD^+, and for collisions between H_3^+ and C forming CH^+ and CH_2^+ at relative collision energies from 60 meV to ∼10 eV. We calibrated the absolute scale of our measured rate coefficients to previous $D_2^+ + C$ measurements.

Our vibrationally cold HD^+ data revealed much higher rate coefficients when compared to previous measurements of Hillenbrandt *et al.* with H_2^+ and D_2^+, carried out using vibrationally excited ions. We attribute this increase in the rates to the absence of vibrational excitation in our studies. Consistent with this interpretation, we observe qualitatively that the measured reaction rates are lower during the first 300 ms of storage, where vibrational cooling is still incomplete. We did not see any significant change in the rates after storage times of 0.5 s, indicating that the influence of rotational excitation on the rate coefficients is not very strong. We find a small preference to form CH^+ over CD^+ a low collision energies, which increases above 1 eV, where the CD^+ channel shows a sharper decrease with collision energy than the CH^+ channel.

To compare our $HD^+ + C$ measurements to theory, we have performed QCT calculations on two newly developed PESs of quartet symmetry. The QCT results agree very well with the experimental rate coefficients for both reaction channels. Furthermore, the experimental CH^+ to CD^+ branching ratio is well reproduced by the QCT calculations up to energies around 5 eV (see Fig. 4 of [77]), where both the experimental as well as the theoretical cross sections for the CD^+ channel become so small that the evaluation of the branching ratio is difficult. Overall, the agreement between experiment and theory is excellent, indicating that this barrierless ion-neutral process can be described and understood using classical arguments.

Furthermore, we have compared the absolute rate coefficients for both $HD^+ + C$ and $H_3^+ + C$ with common capture models, by summing up the rates of both reactive channels in each case. We find that the combined rate coefficients agree reasonably well with capture rates that include both the induced dipole as well as the permanent quadrupole moment of the neutral C atoms, but only after the fraction of reactant states that correlates to reactive surfaces is properly accounted for.

ACKNOWLEDGMENTS

This work was supported by the Max Planck Society. The QCT calculations were performed using HPC resources from GENCI-IDRIS (Grant No. 2023-100538). F.G. and H.K. were supported by the European Research Council under Grant Agreement No. StG 307163. X.U. is a Senior Research Associate of the Fonds de la Recherche Scientifique - FNRS, and acknowledges support under Grant No. 4.4504.10.

[1] E. Herbst, Chemistry in the interstellar medium, Annu. Rev. Phys. Chem. **46**, 27 (1995).

[2] E. E. Ferguson, Ion-molecule reactions in the atmosphere, in *Kinetics of Ion-Molecule Reactions*, edited by P. Ausloos (Springer, Boston, 1979), pp. 377–403.

[3] N. Adams and D. Smith, The selected ion flow tube (SIFT); A technique for studying ion-neutral reactions, Int. J. Mass Spectrom. Ion Phys. **21**, 349 (1976).

[4] I. R. Sims and I. W. M. Smith, Gas-phase reactions and energy transfer at very low temperatures, Annu. Rev. Phys. Chem. **46**, 109 (1995).

[5] I. W. M. Smith, Ion-neutral reaction, in *Encyclopedia of Astrobiology*, edited by M. Gargaud, W. M. Irvine, R. Amils, H. J. J. Cleaves, D. L. Pinti, J. C. Quintanilla, D. Rouan, T. Spohn, S. Tirard, and M. Viso (Springer, Berlin, 2015), pp. 1255–1259.

[6] B. Joalland, N. Jamal-Eddine, D. Papanastasiou, A. Lekkas, S. Carles, and L. Biennier, A mass-selective ion transfer line coupled with a uniform supersonic flow for studying ion-molecule reactions at low temperatures, J. Chem. Phys. **150**, 164201 (2019).

[7] A. Mortada, S. Carles, S. Demes, B. Joalland, F. Lique, A. Benidar, P. Lavvas, and L. Biennier, Kinetics and branching for the reactions of N_2^+ with C_3H_4 isomers at low temperatures and implications for Titan's atmosphere, ACS Earth Space Chem. **6**, 1227 (2022).

[8] S. S. Kumar, F. Grussie, Y. V. Suleimanov, H. Guo, and H. Kreckel, Low temperature rates for key steps of interstellar gas-phase water formation, Sci. Adv. **4**, eaar3417 (2018).

[9] S. Schlemmer, W. Geppert, A. Wolf, J. Glosik, D. Parker, L. Wiesenfeld, H. Kreckel, D. W. Savin, and O. Asvany, Gas phase chemistry, in *Laboratory Astrochemistry* (John Wiley & Sons, New York, 2014), Chap. 3, pp. 109–228.

[10] M. Sablier and C. Rolando, Gas-phase ion-atom reactions, Mass Spectrom. Rev. **12**, 285 (1993).

[11] T. P. Snow and V. M. Bierbaum, Ion chemistry in the interstellar medium, Annu. Rev. Anal. Chem. **1**, 229 (2008).

[12] A. Bergeat and J.-C. Loison, Reaction of carbon atoms, C ($2p^2$, ^{3}P) with C_2H_2, C_2H_4 and C_6H_6: Overall rate constant and relative atomic hydrogen production, Phys. Chem. Chem. Phys. **3**, 2038 (2001).

[13] K. M. Hickson, J.-C. Loison, J. Bourgalais, M. Capron, S. D. Le Picard, F. Goulay, and V. Wakelam, The C(^{3}P) + NH_3 reaction in interstellar chemistry. II. Low temperature rate constants and modeling of NH, NH_2, and NH_3 abundances in dense interstellar clouds, Astrophys. J. **812**, 107 (2015).

[14] K. M. Hickson, J.-C. Loison, and V. Wakelam, Temperature dependent product yields for the spin forbidden singlet channel of the C(^{3}P) + C_2H_2 reaction, Chem. Phys. Lett. **659**, 70 (2016).

[15] K. M. Hickson, J.-C. Loison, and V. Wakelam, Kinetic study of the gas-phase reaction between atomic carbon and acetone: Low-temperature rate constants and hydrogen atom product yields, ACS Earth Space Chem. **7**, 2091 (2023).

[16] V. Plomp, X. D. Wang, F. Lique, J. Klos, J. Onvlee, and S. Y. T. van de Meerakker, High-resolution imaging of C + He collisions using Zeeman deceleration and vacuum-ultraviolet detection, J. Phys. Chem. Lett. **12**, 12210 (2021).

[17] C. C. Havener, M. S. Huq, H. F. Krause, P. A. Schulz, and R. A. Phaneuf, Merged-beams measurements of electron-capture cross sections for O^{5+} + H at electron-volt energies, Phys. Rev. A **39**, 1725 (1989).

[18] C. Havener, M. Nesnidal, M. Porter, and R. Phaneuf, Electron capture by multicharged ions from hydrogen atoms at eV energies, Nucl. Instrum. Meth. Phys. Res. B **56–57**, 95 (1991).

[19] P. C. Stancil, C. C. Havener, P. S. Krstić, D. R. Schultz, M. Kimura, J.-P. Gu, G. Hirsch, R. J. Buenker, and B. Zygelman, Charge transfer in collisions of C^+ with H and H^+ with C, Astrophys. J. **502**, 1006 (1998).

[20] H. Bruhns, H. Kreckel, D. W. Savin, D. G. Seely, and C. C. Havener, Low-energy charge transfer for collisions of Si^{3+} with atomic hydrogen, Phys. Rev. A **77**, 064702 (2008).

[21] H. Kreckel, H. Bruhns, M. Čížek, S. C. O. Glover, K. A. Miller, X. Urbain, and D. W. Savin, Experimental results for H_2 formation from H^- and H and implications for first star formation, Science **329**, 69 (2010).

[22] K. A. Miller, H. Bruhns, J. Eliášek, M. Čížek, H. Kreckel, X. Urbain, and D. W. Savin, Associative detachment of H^- + H→H_2 + e^-, Phys. Rev. A **84**, 052709 (2011).

[23] D. J. McClure, C. H. Douglass, and W. R. Gentry, The dynamics of the reaction D_2^+ + N → ND^++D, J. Chem. Phys. **66**, 2079 (1977).

[24] D. J. McClure, C. H. Douglass, and W. R. Gentry, The dynamics of the reaction D_2^+ + O(^{3}P) → OD^+ + D, and the influence of the atomic quadrupole moment on the cross section at very low kinetic energies, J. Chem. Phys. **67**, 2362 (1977).

[25] G. F. Schuette and W. R. Gentry, The dynamics of the reaction D_2^+ + C → CD^++D at kinetic energies between 0.002 and 14 eV, J. Chem. Phys. **78**, 1777 (1983).

[26] A. P. O'Connor, X. Urbain, J. Stützel, K. A. Miller, N. de Ruette, M. Garrido, and D. W. Savin, Reaction studies of neutral atomic C with H_3^+ using a merged-beams apparatus, Astrophys. J. Suppl. Series **219**, 6 (2015).

[27] N. de Ruette, K. A. Miller, A. P. O'Connor, X. Urbain, C. F. Buzard, S. Vissapragada, and D. W. Savin, Merged-beams Reaction Studies of O +H_3^+, Astrophys. J. **816**, 31 (2016).

[28] P.-M. Hillenbrand, K. P. Bowen, F. Dayou, K. A. Miller, N. de Ruette, X. Urbain, and D. W. Savin, Experimental study of the proton-transfer reaction C +H_2^+→CH^+ + H and its isotopic variant (D_2^+), Phys. Chem. Chem. Phys. **22**, 27364 (2020).

[29] S. Vissapragada, C. F. Buzard, K. A. Miller, A. P. O'Connor, N. de Ruette, X. Urbain, and D. W. Savin, Recommended thermal rate coefficients for the C +H_3^+ reaction and some astrochemical implications, Astrophys. J. **832**, 31 (2016).

[30] P.-M. Hillenbrand, N. de Ruette, X. Urbain, and D. W. Savin, Branching Ratio for O $+H_3^+$ Forming $OH^+ + H_2$ and $H_2O^+ +$ H, Astrophys. J. **927**, 47 (2022).

[31] F. Grussie, A. P. O'Connor, M. Grieser, D. Muell, A. Znotins, X. Urbain, and H. Kreckel, An ion-atom merged beams setup at the cryogenic storage ring, Rev. Sci. Instrum. **93**, 053305 (2022).

[32] R. von Hahn, A. Becker, F. Berg, K. Blaum, C. Breitenfeldt, H. Fadil, F. Fellenberger, M. Froese, S. George, J. Göck, M. Grieser, F. Grussie, E. A. Guerin, O. Heber, P. Herwig, J. Karthein, C. Krantz, H. Kreckel, M. Lange, F. Laux *et al.*, The cryogenic storage ring CSR, Rev. Sci. Instrum. **87**, 063115 (2016).

[33] A. P. O'Connor, A. Becker, K. Blaum, C. Breitenfeldt, S. George, J. Göck, M. Grieser, F. Grussie, E. A. Guerin, R. von Hahn, U. Hechtfischer, P. Herwig, J. Karthein, C. Krantz, H. Kreckel, S. Lohmann, C. Meyer, P. M. Mishra, O. Novotný, R. Repnow *et al.*, Photodissociation of an internally cold beam of CH^+ ions in a cryogenic storage ring, Phys. Rev. Lett. **116**, 113002 (2016).

[34] C. Meyer, A. Becker, K. Blaum, C. Breitenfeldt, S. George, J. Göck, M. Grieser, F. Grussie, E. A. Guerin, R. von Hahn, P. Herwig, C. Krantz, H. Kreckel, J. Lion, S. Lohmann, P. M. Mishra, O. Novotný, A. P. O'Connor, R. Repnow, S. Saurabh *et al.*, Radiative rotational lifetimes and state-resolved relative detachment cross sections from photodetachment thermometry of molecular anions in a cryogenic storage ring, Phys. Rev. Lett. **119**, 023202 (2017).

[35] Á. Kálosi, M. Grieser, R. von Hahn, U. Hechtfischer, C. Krantz, H. Kreckel, D. Müll, D. Paul, D. W. Savin, P. Wilhelm, A. Wolf, and O. Novotný, Laser probing of the rotational cooling of molecular ions by electron collisions, Phys. Rev. Lett. **128**, 183402 (2022).

[36] A. P. O'Connor, F. Grussie, H. Bruhns, N. de Ruette, T. P. Koenning, K. A. Miller, D. W. Savin, J. Stuetzel, X. Urbain, and H. Kreckel, Generation of neutral atomic beams utilizing photodetachment by high power diode laser stacks, Rev. Sci. Instrum. **86**, 113306 (2015).

[37] M. Scheer, R. C. Bilodeau, C. A. Brodie, and H. K. Haugen, Systematic study of the stable states of C^-, Si^-, Ge^-, and Sn^- via infrared laser spectroscopy, Phys. Rev. A **58**, 2844 (1998).

[38] K. A. Miller, H. Bruhns, M. Čížek, J. Eliášek, R. Cabrera-Trujillo, H. Kreckel, A. P. O'Connor, X. Urbain, and D. W. Savin, Isotope effect for associative detachment: $H(D)^- + H(D) \rightarrow H_2(D_2) + e^-$, Phys. Rev. A **86**, 032714 (2012).

[39] Copham Antenna System, Vectorfields Simulation Software, Kidlington, UK.

[40] G4beamline, http://g4beamline.muonsinc.com.

[41] S. Sakai, S. Kato, K. Morokuma, and I. Kusunoki, Potential energy surfaces of the reaction $C^+ + H_2 \rightarrow CH^+ + H$, J. Chem. Phys. **75**, 5398 (1981).

[42] F. Dayou *et al.* (unpublished).

[43] H.-J. Werner and P. J. Knowles, An efficient internally contracted multiconfiguration-reference configuration interaction method, J. Chem. Phys. **89**, 5803 (1988).

[44] P. J. Knowles and H.-J. Werner, An efficient method for the evaluation of coupling coefficients in configuration interaction calculations, Chem. Phys. Lett. **145**, 514 (1988).

[45] S. R. Langhoff and E. R. Davidson, Configuration interaction calculations on the nitrogen molecule, Int. J. Quantum Chem. **8**, 61 (1974).

[46] T. H. Dunning, Gaussian basis sets for use in correlated molecular calculations. I. The atoms boron through neon and hydrogen, J. Chem. Phys. **90**, 1007 (1989).

[47] R. A. Kendall, J. Dunning, H. Thom, and R. J. Harrison, Electron affinities of the first-row atoms revisited. Systematic basis sets and wave functions, J. Chem. Phys. **96**, 6796 (1992).

[48] T.-S. Ho and H. Rabitz, A general method for constructing multidimensional molecular potential energy surfaces from ab initio calculations, J. Chem. Phys. **104**, 2584 (1996).

[49] W. R. Gentry and C. F. Giese, Long-range interactions of ions with atoms having partially filled p subshells, J. Chem. Phys. **67**, 2355 (1977).

[50] G. L. Gutsev, P. Jena, and R. J. Bartlett, Electric quadrupole moments and electron affinities of atoms from H to Cl: a coupled-cluster study, Chem. Phys. Lett. **291**, 547 (1998).

[51] C. Thierfelder, B. Assadollahzadeh, P. Schwerdtfeger, S. Schäfer, and R. Schäfer, Relativistic and electron correlation effects in static dipole polarizabilities for the group-14 elements from carbon to element $z = 114$: Theory and experiment, Phys. Rev. A **78**, 052506 (2008).

[52] N. R. Brinkmann, N. A. Richardson, S. S. Wesolowski, Y. Yamaguchi, and H. F. S. III, Characterization of the X^2A_1 and a^4A_2 electronic states of CH_2^+, Chem. Phys. Lett. **352**, 505 (2002).

[53] P. Halvick and J. C. Rayez, A theoretical study of the dynamics of the reaction $C(^3P) + NO(X\,^2\Pi) \rightarrow CN(X\,^2\Sigma^+) + O(^3P)$, Chem. Phys. **131**, 375 (1989).

[54] D. G. Truhlar and J. T. Muckerman, Reactive Scattering Cross Sections III: Quasiclassical and Semiclassical Methods, in *Atom - Molecule Collision Theory: A Guide for the Experimentalist*, edited by R. B. Bernstein (Springer, Boston, 1979), pp. 505–566.

[55] P. J. Kuntz, Collision-induced dissociation ii: Trajectories and models, in *Atom - Molecule Collision Theory: A Guide for the Experimentalist*, edited by R. B. Bernstein (Springer, Boston, 1979), pp. 669–692.

[56] Z. Amitay, A. Baer, M. Dahan, L. Knoll, M. Lange, J. Levin, I. F. Schneider, D. Schwalm, A. Suzor-Weiner, Z. Vager, R. Wester, A. Wolf, and D. Zajfman, Dissociative recombination of HD^+ in selected vibrational quantum states, Science **281**, 75 (1998).

[57] C. M. Coppola, L. Lodi, and J. Tennyson, Radiative cooling functions for primordial molecules, Mon. Not. R. Astron. Soc. **415**, 487 (2011).

[58] F. von Busch and G. H. Dunn, Photodissociation of H_2^+ and D_2^+: Experiment, Phys. Rev. A **5**, 1726 (1972).

[59] A. R. W. McKellar, W. Goetz, and D. A. Ramsay, The rotation-vibration spectrum of HD: wavelength and intensity measurements of the 3-0, 4-0, 5-0, and 6-0 electric dipole bands., Astrophys. J. **207**, 663 (1976).

[60] H. Kreckel, S. Krohn, L. Lammich, M. Lange, J. Levin, M. Scheffel, D. Schwalm, J. Tennyson, Z. Vager, R. Wester, A. Wolf, and D. Zajfman, Vibrational and rotational cooling of H_3^+, Phys. Rev. A **66**, 052509 (2002).

[61] H. Kreckel, J. Tennyson, D. Schwalm, D. Zajfman, and A. Wolf, Rovibrational relaxation model for H_3^+, New J. Phys. **6**, 151 (2004).

[62] A. Znotins, F. Grussie, A. Wolf, X. Urbain, and H. Kreckel, An approach for multi-color action spectroscopy of highly excited states of H_3^+, J. Mol. Spectrosc. **378**, 111476 (2021).

[63] F. Merkt, K. Höveler, and J. Deiglmayr, Reactions of H_2, HD, and D_2 with H_2^+, HD^+, and D_2^+: Product-channel branching ratios and simple models, J. Phys. Chem. Lett. **13**, 864 (2022).

[64] P. M. Hillenbrand, K. P. Bowen, J. Liévin, X. Urbain, and D. W. Savin, Experimental and theoretical studies of the isotope exchange reaction $D + H_3^+ \rightarrow H_2D^+ + H$, Astrophys. J. **877**, 38 (2019).

[65] K. P. Bowen, P. M. Hillenbrand, J. Liévin, D. W. Savin, and X. Urbain, Dynamics of the isotope exchange reaction of D with H_3^+, H_2D^+, and D_2H^+, J. Chem. Phys. **154**, 084307 (2021).

[66] B. M. Dinelli, S. Miller, and J. Tennyson, Bands of H_3^+ up to $4\nu_2$: Rovibrational transitions from first principles calculations, J. Mol. Spectrosc. **153**, 718 (1992).

[67] C. Lindsay and B. J. McCall, Comprehensive evaluation and compilation of H_3^+ spectroscopy, J. Mol. Spectrosc. **210**, 60 (2001).

[68] D. Talbi, D. J. Defrees, D. A. Egolf, and E. Herbst, Calculations concerning the reaction $C + H_3^+ \rightarrow CH^+ + H_2$, Astrophys. J. **374**, 390 (1991).

[69] R. P. A. Bettens and M. A. Collins, Potential energy surfaces and dynamics for the reactions between $C(^3P)$ and $H_3^+(^1A_1')$, J. Chem. Phys. **108**, 2424 (1998).

[70] R. P. A. Bettens and M. A. Collins, Erratum: "Potential energy surfaces and dynamics for the reactions between $C(^3P)$ and H_3^+ $(^1A_1')$" [J. Chem. Phys. 108, 2424 (1998)], J. Chem. Phys. **114**, 6490 (2001).

[71] D. C. Clary, Fast chemical reactions: Theory challenges experiment, Annu. Rev. Phys. Chem. **41**, 61 (1990).

[72] R. D. Levine, *Molecular Reaction Dynamics* (Cambridge University Press, Cambridge, 2005).

[73] E. Herbst, Gas phase reactions, in *Springer Handbook of Atomic, Molecular, and Optical Physics*, edited by G. Drake (Springer, New York, 2006), pp. 561–574.

[74] G. Gioumousis and D. P. Stevenson, Reactions of gaseous molecule ions with gaseous molecules. V. Theory, J. Chem. Phys. **29**, 294 (1958).

[75] D. McElroy, C. Walsh, A. J. Markwick, M. A. Cordiner, K. Smith, and T. J. Millar, The UMIST database for astrochemistry 2012, Astron. Astrophys. **550**, A36 (2013).

[76] V. Wakelam, E. Herbst, J.-C. Loison, I. W. M. Smith, V. Chandrasekaran, B. Pavone, N. G. Adams, M.-C. Bacchus-Montabonel, A. Bergeat, K. Beroff, V. M. Bierbaum, M. Chabot, A. Dalgarno, E. F. van Dishoeck, A. Faure, W. D. Geppert, D. Gerlich, D. Galli, E. Hebrard, F. Hersant *et al.*, A kinetic database for astrochemistry (KIDA), Astrophys. J. Suppl. Series **199**, 21 (2012).

[77] F. Grussie, L. Berger, M. Grieser, A. Kalosi, D. Müll, O. Novotný, A. Znotins, F. Dayou, X. Urbain, and H. Kreckel, companion paper, Merged-beams study of the reaction of cold HD^+ with C atoms reveals a pronounced intramolecular kinetic isotope effect, Phys. Rev. Lett. **132**, 243001 (2024).